ELSEVIER

International Journal of Mass Spectrometry 216 (2002) 41–57

International Journal of Mass Spectrometry

www.elsevier.com/locate/ijms

The thermal ionization cavity (TIC) source: elucidation of possible mechanisms for enhanced ionization efficiency

David M. Wayne [a,*], Wei Hang [b], Diane K. McDaniel [a,1], Robert E. Fields [c], Eddie Rios [a], Vahid Majidi [b]

[a] *Nuclear Materials and Technology Division, MS E-530, Los Alamos National Laboratory, Los Alamos, NM 87545, USA*
[b] *Chemistry Division, MS K-484, Los Alamos National Laboratory, Los Alamos, NM 87545, USA*
[c] *Materials Science and Technology Division, MS G-770, Los Alamos National Laboratory, Los Alamos, NM 87545, USA*

Received 18 September 2001; accepted 15 January 2002

Abstract

We discuss the ionization efficiency performance of a thermal ionization cavity source which has been adapted for use in an orthogonal acceleration linear thermal ionization cavity time-of-flight mass spectrometer (TIC-TOFMS). Our results indicate that the maximum ionization efficiency of thorium, a notoriously difficult element to ionize thermally, in the present TIC-TOFMS system is about 1–3%. This represents a 10–30× enhancement of the typical Th sample utilization for conventional, Re filament-based, thermal ionization mass spectrometry sources. Thorium samples were small (0.075–25 ng), therefore, analytical blanks for Th in the tungsten TIC were also measured and subtracted from the total Th ion signal arriving at the detector. Prominent peaks that correspond to multiply-charged (2^+ and 3^+) tungsten ions are always evident in high-temperature (>2400 °C) spectra. Furthermore, TIC-TOFMS spectra also contained peaks corresponding to elements with ionization potentials in excess of 8 eV, such as beryllium. The presence of multiply-charged tungsten peaks, and beryllium peaks, are indicative of significant ionization via non-thermal processes, such as electron impact, in or near the TIC. (Int J Mass Spectrom 216 (2002) 41–57) © 2002 Published by Elsevier Science B.V.

Keywords: Thermal ionization cavity; Isotope separators; Saha–Langmuir equation; Thermal ionization mass spectrometry; TOFMS; Thermal ionization efficiency; Thorium; Metal clusters

1. Introduction

Thermal ionization cavities (TICs) have been used for over three decades as ion sources for large scale isotope separators [1–7]. The early cavity-type ion sources were relatively simple in design, and consisted of a cylindrical, hollow tungsten crucible topped by a removable cap with a central ion extraction orifice [3]. These devices were heated via electron bombardment to about 3250–3300 °C. Early studies [1–3,8,9] showed that ionization efficiencies (i.e., the ratio of the number of atoms captured—or ions detected—to the number of atoms loaded) for cavity-type ion sources were much greater than those obtained from ribbon-type ion sources, particularly amongst the rare earths. Using a modified TIC ion source, Pilzer and Engler [10] obtained ionization efficiencies >95% for both Ce and Tb.

* Corresponding author. E-mail: d-wayne@lanl.gov
[1] Present address: University of Maryland, Department of Geology, College Park, MD 20742-4211, USA.

1387-3806/02/$ – see front matter
PII S1387-3806(02)00551-1

Enhancements in ionization efficiency also extended to refractory elements such as U and Th. The ionization efficiencies for U and Th in conventional rhenium single filament and multiple filament ion sources for thermal ionization mass spectrometry (TIMS) are typically between 0.01 and 0.5% [11–14]. Using tungsten crucibles, two teams [1–3] documented ionization efficiencies between 9 and 20% for U, and ∼5.2% for Th. Kirchner [15] later observed ionization efficiencies between 15 and 39% for uranium in a rhenium cavity.

During the early 1980s, Cesario et al. [16] adapted a magnetic sector instrument so that it could accommodate both the TIC source, and a conventional resistively heated filament source. For the TIC experiments, they electrodeposited samples onto the tip of a sharpened tantalum rod (o.d. ∼1 mm). The rod was fastened to a sample holder and inserted into a rhenium tube (o.d. ∼2 mm), which was heated by electron bombardment. The distance between the tip of the Ta rod and the orifice of the enclosing Re tube was controlled by means of a screw at the base of the sample holder. Although the Re tube was fixed relative to the electron bombardment filament, ion current increased as the distance between the tip of the Ta rod and the orifice of the Re tube decreased. Cesario et al. [16] obtained 4–28× greater ion yields (0.02–0.143% per atom) for 40–300 ng of uranium, relative to similar samples run using a conventional Re filament source (filament U ion yield = 0.005% per atom).

Duan et al. [17] developed a simpler TIC source: a cylindrical cavity (∼0.02 cm diameter, ∼1.25 cm depth) drilled into a length of high-purity (>98.5%) tungsten rod stock (0.15 cm o.d.). The advantage of this design is that samples can be loaded directly as particulates (e.g., high purity metal oxides and/or silicates), or as solution droplets dried on to a length of wire. Heating was accomplished by electron bombardment. The TIC was affixed to a direct insertion probe (DIP) mounted on a movable stage. Thus, TIC position can be controlled by moving the DIP, and by adjusting the stage. Though the TIC was not tested in a magnetic sector MS, enhanced ion yields for uranium, thorium, zirconium and several lanthanides were obtained using an isotope separator [17]. Duan and co-workers [17,18] also obtained similar results for uranium and several lanthanides using quadrupole MS. Ion yields for Pu in the quadrupole TIC MS [18] were comparable to those obtained via conventional TIMS in a magnetic sector instrument [19]. The thermal ion source used in the TOFMS studies described here, and in a previous study [20], represents a further refinement of the ion source developed by Duan and co-workers [17,18].

The significance of previous work on the TIC source [16–20] becomes clearer when one considers the absolute number of atoms being measured during TIMS analysis. For a conventional filament ion source, detection limits in magnetic sector TIMS are on the order of 10^4 to 10^6 ions. The use of the TIC source, with a potential 10–100-fold improvement in ionization efficiency, could lower detection limits to 10^2 to 10^4 ions for many elements, provided that exceptionally low background levels can be maintained. In order to achieve reliable measurements at these extremely small concentration levels, the analytical blank for the element(s) in question must also be rigorously characterized.

Previous work on TIC-sourced MS involved the analysis of milligram- to microgram-sized samples and, therefore, the issue of analytical blanks was not addressed. Our results are exclusively from thorium samples in the 25 ng–25 pg range, which necessitated a thorough investigation of the Th background and analytical blank in the TIC source. To provide a basis for comparison, we summarize previous work on ionization in hot cavities, and the ionization behavior of thorium in the context of conventional TIMS analysis. Finally, we present the results of an ionization efficiency study using the TIC source, based on TOFMS measurements.

2. Background

2.1. Theoretical considerations

The theoretical basis for thermal ionization within an enclosed volume has been discussed previously

[4,5,8,9,15,21,22]. Though there was some disagreement as to the nature of ionization within a cavity [15,22], a consensus has been reached in recent years [7]. Ion emission, α, from a hot surface can be described by the Saha–Langmuir equation:

$$\alpha = \frac{n_i}{n_0} = \left(\frac{\sigma_i}{\sigma_0}\right) \exp\left[\left(\frac{\varphi - W_{iZ}}{kT}\right)\right], \quad (1)$$

where n_i/n_0 is the ion/atom ratio, (σ_i/σ_0) the ratio of the statistical weights of the ionic and ground states, φ the work function of the ionizing surface, W_{iZ} the first ionization energy of an element Z in the sample, k Boltzmann's constant and T is the surface temperature in Kelvin. The surface ionization efficiency is given by

$$\beta = \frac{n_i}{(n_i + n_0)} = \frac{\alpha}{(1+\alpha)}. \quad (2)$$

Early investigators [1–3] working with cavity-sourced isotope separators first observed that ionization efficiencies were significantly higher than those predicted by Saha–Langmuir, and decreased sharply when ionizer temperature fell below ~3000 K. Latuszynski and Raiko [21] observed that ionization efficiency also decreased when the total extracted ion flux (sample ions + impurity ions + ions from the ionizing surface) exceeded $\sim 10^{-5}$ ions/cm^2. They derived an equation describing thermal ionization in a cavity based on the flow of thermionic electrons and surface-ionized atoms between the cavity wall and the cavity volume, regulated by a plasma sheath. Kirchner and co-workers [5,7,15], and Afanas'ev et al. [8] argued that such behavior could be explained purely by surface ionization within the cavity, enhanced by a factor proportional to the ratio (κ) of the cavity's inner surface area to its orifice area and moderated by the probability (ω) of an ion leaving the cavity. The κ factor fixes the number of wall collisions an atom may experience prior to leaving the cavity. The calculation of η_Z for a single element (Z) in a multi-element vapor, $\sum_Z n_{iZ}$ (the 'modified Saha-equation' #14 in [8]) is

$$\frac{[(\eta_Z/1-\eta_Z)]\eta_{avg}}{1+\eta_{avg}} = \left(\frac{2\sigma_{iZ}}{\sigma_{0Z}}\right)\left(\frac{2\pi m}{h^2}\right)^{3/2} P^{-1}(kT)^{5/2}\left[\exp\left(\frac{-W_{iZ}}{kT}\right)\right], \quad (3)$$

where P is the total pressure, η_{avg} the average ionization efficiency of the plasma, m electron mass, and h is Planck's constant. Assuming quasi-neutrality, and simplifying using the laws of Boltzmann, Richardson and Saha–Langmuir, Eq. (3) becomes [15]

$$\eta_Z = \frac{\beta_Z \omega\kappa}{1 - [\beta_Z(1-\omega\kappa)]}. \quad (4)$$

Eq. (4) approaches $\eta_Z/\beta_Z = \omega\kappa$, for $\beta_Z \ll 1$.

By contrast, Huyse [22] attributed the difference between the surface ionization efficiency (β), and the cavity ionization efficiency (η), to the plasma sheath. As electrons (or ions) are emitted from the hot cavity surface, the surface becomes positively (or negatively) charged relative to the plasma. For a tungsten cavity, electrons are lost from the walls which then become positively-charged. The positively-charged walls attract a sheath of electrons. Tungsten ions liberated from the surface move into the cavity volume. More tungsten ions are produced until the wall potential is screened by the electron sheath, and the plasma in the cavity volume becomes quasi-neutral. The ion-to-neutral ratio in the plasma is related to that at the walls by

$$a_v = a_s \exp\left(\frac{e\Phi_p}{kT}\right), \quad (5)$$

where Φ_p is the plasma sheath potential (=0 at the wall), a_v the ratio of ions to neutrals in the plasma, and a_s is the same ratio at the cavity wall. The relation between the thermal ionization efficiency in the volume (η) and surface ionization efficiency near the wall (β) becomes

$$\eta = \left[\frac{\beta \exp(-e\Phi_p/kT)}{(1-\beta(1-\exp(-e\Phi_p/kT)))}\right]. \quad (6)$$

In an impure system, the plasma sheath potential is fixed by the element with the greatest surface ion density. Readily ionizable elements, such as K^+ and Na^+, can strongly influence the sheath potential at lower temperatures where contributions from the ionizer are small.

In response to the Huyse model, Kirchner [15] pointed out that the plasma sheath model may work only for a system in which $T_{\text{electron}} = T_{\text{ion}}$, and provided evidence that the TIC plasma was not likely to be in thermal equilibrium. He then plotted experimentally-observed, and calculated, ionization efficiencies for several elements vs. their first ionization potential. The resulting curves best fit Eq. (4) for $\omega\kappa = 150$, well away from the thermal equilibrium value of 7500. Kirchner's parametric studies [15] further attribute some degree of ionizer material dependence to total ionization efficiency, and supports increased ionization efficiencies at higher temperatures and at greater neutral densities.

The studies summarized above attribute 100% of the tungsten ion current to the vaporization and ionization of tungsten atoms via thermal processes, such as surface ionization. The results of this study indicate that this is not the case, and that the role of non-thermal ionization processes, such as electron impact, may be far more significant than previously thought. The development of realistic predictive models for ionization efficiency in cavity-type sources heated using electron bombardment must take non-thermal processes into account.

2.2. Thorium ionization efficiency

The ionization behavior and efficiency of thorium (Th) in thermal ionization mass spectrometry is very well-documented (Table 1, and references therein). In the geosciences, ^{238}U–^{234}U–^{230}Th–^{232}Th systematics are used to investigate recent (<500,000 years before present) geological processes [14,23–26], and to obtain radiometric ages on a variety of geological materials [13,27–30]. To facilitate the analysis of miniscule (<100 pg) quantities of Th in corals, cave deposits, sea-floor basalt, and other materials,

Table 1
Summary of thermal ionization efficiency data for Th

	Surface type	Th (% ionization efficiency)[a]	Concentration range (atoms)
Predicted from Saha–Langmuir equation ($T = 2200\,^{\circ}$C)			
	Ta ($\varphi = 4.25$)[b]	0.019	
	W ($\varphi = 455$)[b]	0.076	
	Re ($\varphi = 4.98$)[b]	0.570	
	Re ($\varphi = 5.75$)[c]	17.5	
	Re ($\varphi = 5.36$)[d]	3.30	
TIC-TOFMS (this study)		1.1–3.0	6.5×10^{11} to 1.3×10^{14} (25 pg–5 ng)
TIC-separator [17]		2	$\sim 2.6 \times 10^{18}$ (1 mg ThO_2)
Filament TIMS			
[13][e]		0.07–0.13	$<10^{12}$ (~40 pg)
		~0.05	$>10^{12}$, $<10^{13}$
		~0.01	$\sim 10^{14}$ (~4 ng)
		~0.002	5×10^{14} (~20 ng)
[14][f]		0.04	1.3×10^{14} to $\sim 10^{15}$ (50–400 ng)
[32][g]		4–6	2.6×10^{11} to 7.8×10^{11} (100–300 pg)
[38][h]		0.11–0.41	6.5×10^{13} to 6.2×10^{15} (25–2400 ng)

[a] Based on $W_{iZ} = 6.08$ for Th.
[b] Work function (φ) for polycrystalline material.
[c] φ for single crystal.
[d] Estimated φ for carburized Re (see text).
[e] Single Re filament.
[f] Triple Re filament.
[g] Single carburized Re filament.
[h] Double Re filament, run using cw-RIMS.

geochemists have sought to improve sample utilization by enhancing Th ionization efficiency during mass spectrometric analysis.

For conventional single rhenium (Re) filament TIMS, thorium ions first emit at ∼1800 °C. Data is collected between 1810 and 1870 °C [13,14,23]. At 1850 °C, the Saha–Langmuir equation predicts an ionization efficiency of 0.02% for Th (first ionization potential = 6.31 eV) on a polycrystalline Re surface (φ = 4.72 eV). Carburization increases the work function of a Re surface by ∼0.4 eV [31], and the predicted ionization efficiency at 1850 °C to ∼0.15%.

Using a single Re filament, Edwards et al. [13] observed maximum ionization efficiencies of 0.07–0.13% for 1×10^{11} to $\sim 5 \times 10^{12}$ thorium atoms (0.04–2 ng Th). Significantly, they observed a systematic decrease in Th ionization efficiency with increasing sample size (Table 1). Later, Goldstein and co-workers [14,23] used a triple filament assembly that permitted higher ionization temperatures (>2100 °C). They observed significant enhancements in Th ionization efficiency (to 0.04%) for large Th loads (50–400 ng). Esat [32] reported a "combined transmission and ionization efficiency" of 4–6% for 0.1–0.3 ng Th samples loaded onto a single, carburized Re dimple filaments.

Esat [32] attributes the >30× increase in ionization efficiency to careful sample and filament preparation, and to the thorough carburization of the Re surface prior to sample loading. In terms of the Saha–Langmuir formalism, part of the 30-fold increase in Th ionization efficiency can be attributed to the increase in work function due to the carburization of the Re surface. However, Saha–Langmuir predicts an increase in Th ionization efficiency from ∼0.15 to ∼0.38% for a carburized Re surface between 1850 and 2000 °C. Thus, some other process may account for the further enhancement of Th ionization.

Duan et al. [17], using milligram quantities of pure Th oxide in a tungsten TIC, obtained an ionization efficiency of ∼2% for an isotope separator. Assuming an ionizer temperature of ∼2200 °C, Saha–Langmuir predicts an ionization efficiency of ∼0.03% for Th on a polycrystalline W surface. Thus, the observed ionization efficiency enhancement is ∼65× for Th in the cavity source, relative to the predicted value obtained from a flat tungsten surface.

3. Materials and equipment

3.1. Thermal ion source and power supply

A detailed description of the apparatus used in this study is provided elsewhere [20]. The ion source (Fig. 1) consists of a tantalum electron emission filament, and mounting posts, inside a cylindrical electron shielding can, a base plate, two ion focusing plates, and various insulators, connectors and screws. The first focusing plate has a circular orifice (0.25 cm diameter) for ion transport, and the second has a rectangular orifice (0.13 cm wide × 0.51 cm long) to optimize beam shape. Emission current is provided to the tantalum filament by a low voltage, high current power supply (HP 6641, Hewlett-Packard Co., Rockville, MD, USA), and the can potential and floating potential are provided by a high voltage power supply (AU-5R60, Matsusada Precision Inc., Japan) operated via an isolation transformer.

Tungsten cavities were fabricated by drilling a cylindrical hole approximately 10 mm deep, and 0.25 mm in diameter, into a 40 mm length of >98.5% tungsten wire (o.d. = 1.5 mm, Whitmor Wirenetics Inc., Valencia, CA, USA). The TIC is fastened to the tip of a DIP held at ground potential during the experiment. The TIC holder is fastened to the DIP by a threaded alumina coupling, which prevents conductive heat loss to the rest of the system. Cavities are pre-treated prior to use by heating in the source region for 5–10 min in vacuo to >2500 °C. Cavity temperature was monitored using a rack-mounted optical pyrometer (QL1200C, Quantum Logic Corp., Westport, CT, USA) focused on the TIC tip.

Alumina insulators on the support posts are replaced every 3–5 days to remove vapor-deposited metal films which can short the electron shielding can voltage (2.5 kV) to the focusing plates. Electron emission

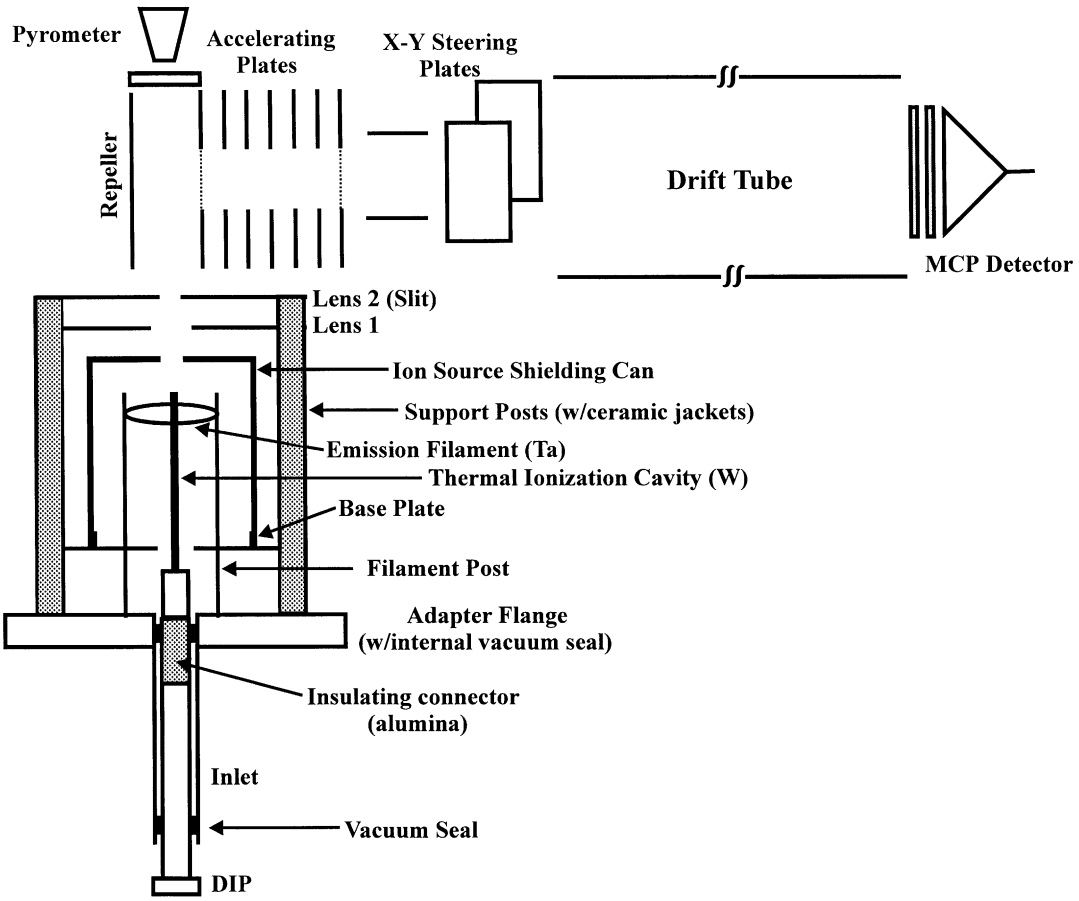

Fig. 1. Schematic diagram of the TIC-TOFMS system. The electronic feedthroughs and vacuum ports are not shown.

filaments and ion source components are also replaced at this time.

3.2. Time-of-flight mass spectrometer

The orthogonal acceleration time-of-flight mass spectrometer (oa-TOFMS) is a commercial, linear, 1 m instrument (C-677, R.M. Jordan Co., Grass Valley, CA), with two grids, and two acceleration stages for spatial focusing. Typical operating parameters are listed in Table 2. The detector consists of two chevron-mounted, 25 mm, high-gain ($\sim 10^6$) microchannel plates with sub-nanosecond response time. The duty cycle of the TOFMS is ~1.9% for Th ions with average ion energy of ~1 eV [6], at a 1333 Hz repeller frequency, and 1.27 cm aperture diameter. Time-resolved mass spectra were collected using an 8-Bit Tektronix digital oscilloscope (TDS 520C, Tektronix Measurement Group, Portland, OR). Peak intensities (in volts) are measured across the 50 Ω impedance of the digitizer. An IBM-compatible computer with an Intel Pentium III microprocessor and LabView software (Version 5.0 for Windows 95, National Instruments, Inc., Austin, TX, USA) was used for acquiring the spectra in numerical form.

3.3. Sample preparation

All data for this study were obtained by serially diluting a commercially-manufactured, high-purity

Table 2
Linear TIC-TOFMS operating conditions

TIC source	
Repeller frequency	1333 Hz
Repeller voltage	+230 to +310 V
Floating potential	−2500 V
Emission current (mA)	Th: 28–35
Acceleration potential	3000 V
Mass spectrometer	
Ion optics	
Lens 1	−150 to −400 V
Lens 2	−450 ± 50 V
X	−2850 ± 50 V
Y	−3200 ± 100 V
Grid	<1 V
MCP detector	−2000 V
Detector gain	4×10^6
Flight tube pressure	4×10^{-8} (at rest) to 5×10^{-7} Torr (in operation)

10.00 ± 0.05 ppm thorium nitrate solution (Lot #917410, High Purity Standards, Charleston, SC, USA). New batches of the dilute Th solutions were made weekly. Microliter quantities of these solutions were loaded onto the tip of a length of tungsten wire (0.127 mm, o.d.) which had been previously coated with a small quantity of colloidal graphite ('Aquadag', Ted Pella, Inc., Redding, CA, USA). The nitrate solution droplet was partially dried, converted to chloride form by the addition of 2.0 μL of 3.75% HCl (diluted with Milli-Q water from 'Seastar' grade HCl), and then dried completely under a heat lamp. A final coating of colloidal graphite was applied by passing the sample through a wire loop containing a thin film of the liquid Aquadag suspension. The sample was then re-dried, inserted into the cavity and cut to a minimum length using the extent of the Aquadag coating as a marker. The cavity was loaded into the sample chamber, and heated gently (1–2 mA electron current) for ∼30 min to degas the sample and reduce the thorium chloride to thorium metal.

3.4. Sample heating and impurity peaks

Run conditions for Th were achieved within 2 h after sample insertion. If the cavity temperature is raised

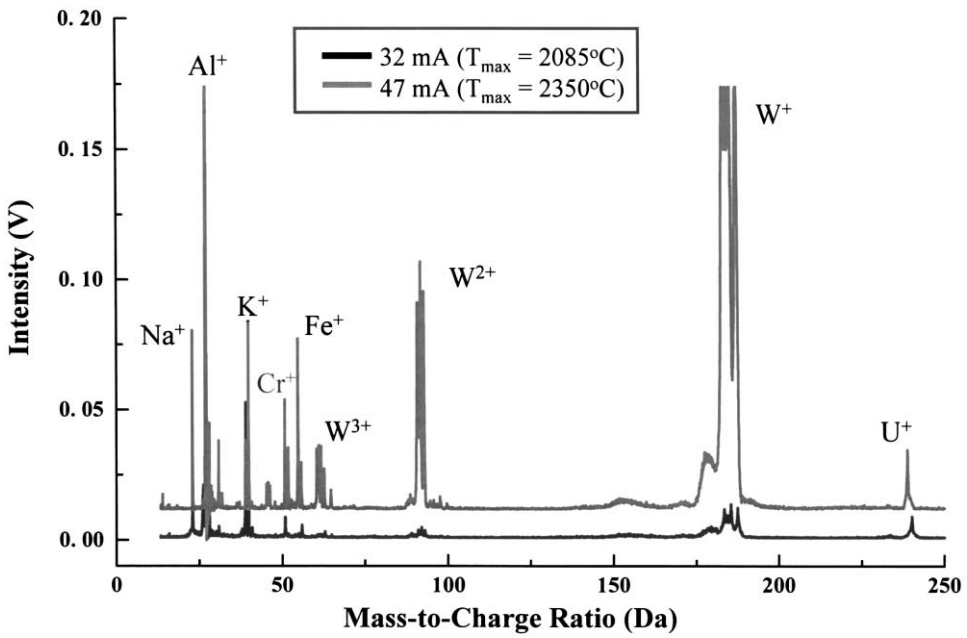

Fig. 2. Mass spectrum obtained by heating an empty tungsten TIC to 2085 °C (bottom trace) and to 2350 °C (top trace). A prominent uranium peak was observed for every empty TIC heated to ≥1900 °C. Note also the multiply-charged tungsten peaks.

too quickly, the ion beam is rendered unstable by the explosive release of gaseous constituents. At the typical operating conditions for thorium ion emission, the total power deposited on the cavity is about 30 ± 3 W. All Th samples loaded with colloidal graphite exhibited complete conversion from Th nitrate to Th metal during pre-heating. A thorium oxide peak was observed in only one run over the course of this study. The presence of the ThO^+ peak is not problematic, as Th^+ and ThO^+ data can be collected simultaneously on the TOFMS.

When an electron current of 1.5–2 mA was established between the Ta filament and the TIC, intense (0.5–1 V) Na^+ and K^+ peaks were observed. The intensity of these peaks first rises, and then decreases, as the current and cavity temperature increases. Calcium and barium peaks of moderate intensity (50 mV to >1 V) appeared at 5 mA (Ca) and 8 mA (Ba) and persisted to ~10 mA (Ca) to 15 mA (Ba) (~1300–1600 °C). At ~15–17 mA (1600–1700 °C), low- to moderate-intensity (~10–60 mV) rare earth (La, Ce, Nd) peaks appeared, which persisted to ~22–23 mA (1850–1950 °C). A persistent uranium peak was also observed in all runs above ~1950 °C. Other commonly observed impurities include Fe, Al, and Sr. Of all the impurity peaks observed at lower temperatures, only Na^+, Al^+, K^+, and Fe^+ persist to the operating temperatures required for Th^+ ion emission (Fig. 2). At high temperatures, peaks corresponding to W^{3+}, W^{2+} (second ionization potential = 17.7 eV), W^+ (first ionization potential = 7.864 eV), and U^+ were present during all runs (Fig. 2).

Results of numerous analytical blanks indicate that the alkali and alkaline earth impurities in the W rod used to fabricate the TICs are ubiquitous. Relative intensities of the calcium and barium peaks suggest that they were also present in the Milli-Q water. The rare earth impurities (and considerable Ba) were present in the Aquadag. Tungsten metal peaks, also observed previously [17,18], appear at >2200 °C, as do multiply-charged tungsten species (Fig. 2). The nature of the uranium peaks is discussed below.

4. Results

4.1. Thorium analyses

Thorium samples (Table 3) were run at the following loadings: 25, 2.5, 1.25, 0.25, 0.125, and 0.075 ng. We made several attempts to run a 0.025 ng sample, though the number of ions detected during these runs was never appreciably greater than the corresponding Th blank. For ionization efficiency determinations (Fig. 3), the temperature was increased until either the thorium peak, or the uranium blank peak, appeared at ~1900–2000 °C. The LabView-based data collection program was then initiated, and temperature was

Table 3
Thorium ionization efficiency data

Th loading (ng)	Time (min)	Th ions	%IE
0.075	30.4	2.13E + 08	1.95
0.125	42.1	1.20E + 09	1.65
	41.6	1.13E + 09	1.55
	45.3	5.11E + 08	0.70
	47.9	9.70E + 08	1.34
0.25	13.5	5.57E + 08	1.53
	23.5	4.91E + 08	1.35
	35.5	6.54E + 08	1.80
	23.2	2.30E + 08	0.63
	45.2	4.19E + 08	1.15
	15.8	4.04E + 08	1.11
1.25	50.5	2.51E + 09	1.38
	52.4	1.18E + 09	0.65
	58.2	7.37E + 08	0.41
	63.2	1.04E + 09	0.57
	36.0	2.60E + 09	0.41
	61.7	2.17E + 10	2.99
	50.1	7.48E + 09	1.03
	45.3	7.56E + 09	1.04
2.5	48.7	5.64E + 09	1.55
	30.6	6.14E + 09	1.69
	34.1	3.05E + 09	0.84
	42.8	2.78E + 09	0.77
	61.5	3.48E + 09	0.96
	63.2	3.87E + 09	1.07
25	70.8	1.84E + 10	0.51
	57.8	9.08E + 09	0.25
	47.1	5.60E + 09	0.15
	33.2	4.59E + 10	0.32
	64.1	1.73E + 11	1.19

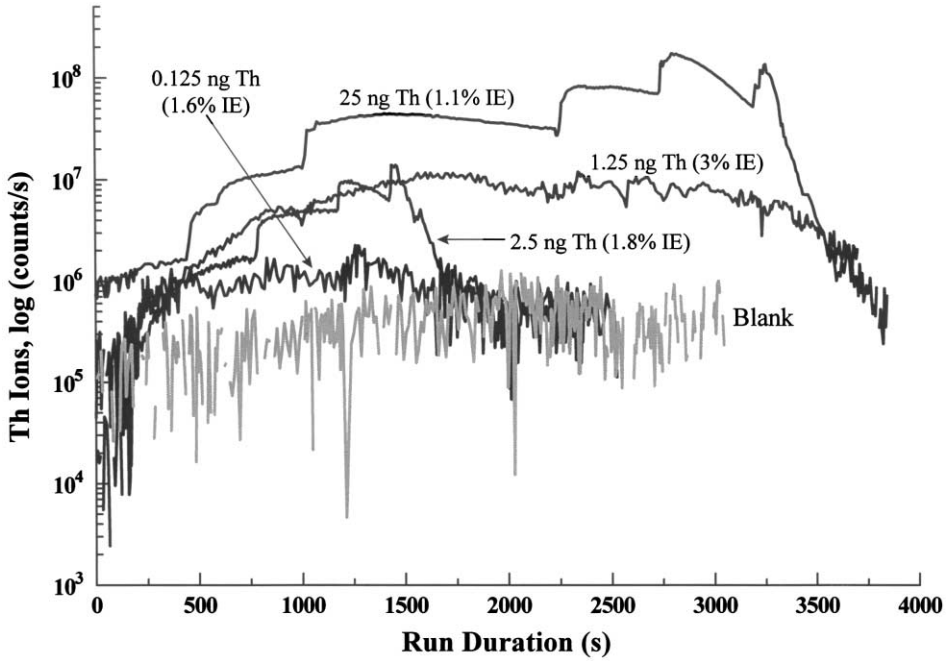

Fig. 3. Time–thorium ion signal intensity profiles (note log scale) obtained from TIC ionization efficiency experiments for a range of thorium concentrations. The sharp discontinuities are the result of step-wise increases in ionizer temperature. The total area under these profiles was used to calculate ionization efficiency. Profile for Th blank is in gray.

increased in a stepwise fashion when the Th ion signal reached a discernible plateau. Temperature increases correspond to the step-like discontinuities in the peak intensity profiles (Fig. 3). During data collection, peak shape and peak intensity were continuously monitored, and focusing adjustments were made to compensate for any losses. Though the TIC-TOFMS is capable of mass resolution (M/ΔM, at FWHM) of >800 [20], the ion source and TOFMS focusing voltages were set for maximum ion transmission. Thus, the effective mass resolution during the Th ionization efficiency measurements was less than optimal (>300–500).

First emission temperature and maximum peak intensity correlated positively with increasing thorium concentration. For the 25 ng runs, thorium first appears at temperatures of ∼1950–1980 °C. For the 1.25 ng runs, the thorium signal first appeared at 2050–2115 °C, and for the 0.25 ng runs Th did not appear until the temperature reached ∼2200 °C. The maximum peak intensity for a 25 ng run, 650 mV (= 3.25×10^{-9} A, assuming a detector gain of 4×10^6), was attained at an average temperature of 2420 °C. Intensities for 1.25 and 2.5 ng Th runs reached maxima of 35–50 mV, while the maximum intensities for 0.125–0.25 ng Th runs were ≤5 mV (Fig. 4). Run duration (Table 3) was minimized in order to minimize the blank contribution. Runs tended to last longer for larger loads (25 ng Th: ∼33–71 min), relative to smaller loads (0.25 ng Th: ∼14–45 min).

Most of the Th data were collected between 2200 and 2400 °C. The endpoint temperature was ≥2500 °C (55–57.5 mA electron current). At the endpoint temperature, the sample was run until the Th signal intensity observed for the sample in question approximated that of the most recent blank at the same temperature, typically 1–2 mV (Fig. 4).

After ∼60–80 min of operation at high temperatures (≥2200 °C), we observed a slow, but steady, degradation in thorium signal intensity and peak

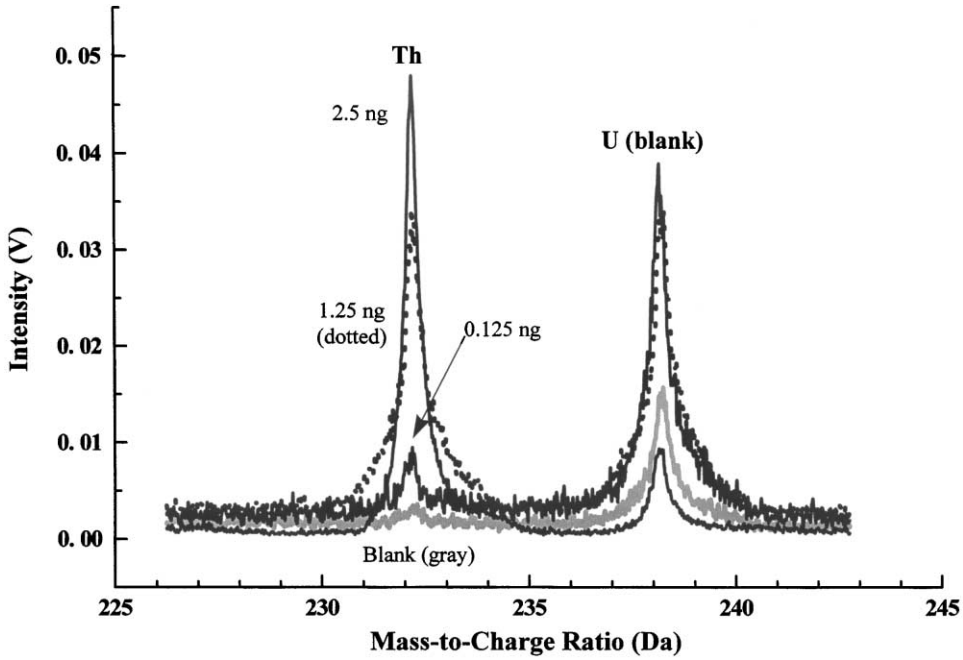

Fig. 4. Thorium profiles obtained from TIC ionization efficiency experiments for a range of concentrations. The maximum thorium blank is gray, and the 1.25 ng thorium profile is represented by a dotted line, for contrast. The uranium peak at $m/z = 238$ is present during each run, and is the result of a uranium impurity (blank) in the TIC itself. Variations in the uranium blank are real, and reflect differences in cavity temperature (at the time the data was collected), and the amount of time a cavity has spent at temperatures of ~1900 °C, or greater.

shape that could not be corrected by beam focusing, or by repositioning the TIC within the ion source. The degeneration of peak shape and intensity corresponds to the accumulation of electrically-conductive, vapor-deposited metal films on the insulating support posts that hold the focusing plates and the ion source shielding can (Fig. 1). The shielding can floats at 2500 V, and typical focusing plate potentials are ≤500 V (Table 2). As the stainless steel ion source components vaporize, metal films deposit on the support posts. Eventually, the potential carried by the metal-coated posts exceeds the focusing plate voltages. Consequently, proper focusing is no longer possible.

4.2. Thorium and uranium analytical blanks

Early ionization efficiency evaluations using TIC sources in isotope separators were performed by running gram quantities of material [1–3]. The initial quadrupole MS studies [17] used milligram quantities of pure oxides. Cesario et al. [16] and Duan et al. [18] used analyte loadings in the 2–0.04 μg range. For experiments on neptunium and plutonium, however, Duan et al. [18] were able to work with samples as small as 0.01 ng. None of these studies incorporated an assessment of the analytical blank. We have undertaken a careful assessment of the analytical blank contribution from the TIC source, and all materials used to carry the sample, because we are interested in the analysis of small quantities (≤25 ng) of Th.

This study was originally intended to assess the ionization efficiencies of both uranium and thorium in the TIC source. However, prominent and persistent uranium peaks were observed during the pre-treatment of empty cavities (Fig. 2), as well as during blank and Th IE runs (Fig. 4). The uranium peak first appears at ~1900–2000 °C, and increases in intensity to

75 ± 25 mV at higher temperatures (~2200–2300 °C). The maximum intensity of the uranium peak decreases to $\sim 15 \pm 5$ mV in cavities which are used more than two or three times. Analyses of thorium solutions using magnetic sector ICPMS revealed no U impurities above detection limits (~30 ppt). Using the same technique, trace amounts of uranium (0.60 ± 0.06 ppm) and thorium (1.2 ± 0.1 ppm) were detected in the tungsten rod stock used to fabricate the TICs.

The appearance of a relatively strong uranium peak at relatively low temperatures ruled out further study of uranium ionization efficiency in the TIC. A small (<1 mV), but measurable, Th peak typically appears at ~2300 °C (45 mA electron current). Although thorium contents may be 2× greater than uranium in the TIC, unlike uranium, the thorium contribution from the TIC is significant only at very high temperatures ($\leq$2 mV at $T \geq 2500$ °C). This disparity may be due, in part, to the lower melting temperature of uranium (1132 °C) relative to thorium (1842 °C), and to the solution behavior of both elements in tungsten.

Thorium blanks were measured by running 2.5 μL of distilled, de-ionized water ('Milli-Q' water) in the same manner described for Th above. For Th concentrations below 25 ng, one blank was run per sample and the blank contribution to the peak at $m/z = 232$ was calculated and subtracted from the subsequent sample run. For loadings between 0.075 and 0.25 ng, the Th blank constituted between 13 and 40% of the total Th signal. At 2.5 ng Th, the blank was <15% of the total Th signal. At 25 ng Th, the blank was <9% of the total Th signal. All ionization efficiency data presented here are corrected for the Th analytical blank.

A new ionization cavity was substituted after two or three Th samples, each with the same concentration, were run. No increase in the Th blank was observed after the same TIC was used for repeat ionization efficiency determinations at a given concentration. Multiple (two to four) Th analyses at a single concentration level were also performed in the same ion source without cleaning. Again, we observed no systematic increases in the Th blank signal from successive blank runs in the same ion source. Though the re-use of TICs and ion source components had no impact on ionization efficiency measurements, we do not recommend re-use of the TICs or electron shielding cans when performing quantitative or isotopic analyses.

4.3. Data collection and processing

Ionization efficiency was calculated by integrating Th peak area over time elapsed from its first appearance to its exhaustion (to blank levels). To approximate the number of ions arriving at the detector, Th peak area was converted to total charge using the equation

$$Q_R = \frac{N[(A/eRg)]}{D}, \quad (7)$$

where Q_R corresponds to the 'real' total charge arriving at the detector, N is the number of ion packets arriving at the detector per second (= inverse of the repeller frequency), A the time-integrated area of the Th peak, e the charge on a single ion (1.6×10^{-19} C), R the impedance of the transient digitizer (=50 Ω), g corresponds to the detector gain (~10^6), and D is the TOFMS sampling duty cycle. The total charge, Q_R, corresponding to each reading of the Th peak was then integrated over time (in seconds) to obtain the total number of positive charges (Th ion equivalents) detected over the duration of the run. This number was then divided by the number of Th atoms loaded to obtain the percent ionization efficiency.

Ionization efficiency data for Th (in percent) are presented in Table 3. Maximum ionization efficiencies at each thorium concentration vary from 1.19% (25 ng) to 2.99% (1.25 ng). These results are similar to those determined previously [17] for the TIC mass spectrometry source, loaded with milligram quantities of thorium dioxide, in an isotope separator.

5. Discussion

5.1. Ionization mechanisms

All elements can be, to some degree, thermally ionized. However, the ionization efficiency of elements with first ionization potentials greater than

~6.3 eV is typically <1% [15]. Elements with first ionization potentials greater than ~8 eV (such as P, N, Be, etc.) may undergo some thermal ionization, but are more efficiently ionized by other mechanisms, such as electron impact (EI). We performed two very simple experiments confirm or deny the possibility of EI within, or near, the TIC. At an emission current of ~10 mA, we bled room air into the ion source housing by loosening the locking cap that holds the DIP in place. Immediately, very intense (>1 V) N^+ and $(N_2)^+$ peaks appeared in the mass spectrum. In the second experiment, the emission current was set to ~45 mA, and several elemental peaks (K^+, Al^+, Fe^+, and W^+) were observed. With the oscilloscope in "peak detect" mode, the emission current was then switched off. With no emission current, only a small K^+ peak remained in the mass spectrum. These two crude experiments suggested that electron impact processes within, or adjacent to, the TIC were more significant than first thought.

Fig. 5 shows a mass spectrum obtained from a 2.5 μL droplet of 10 ppm mixed element mass spectrometry calibration solution that contains beryllium (Spex "Claritas PPT" Multi-Element Solution 5, Spex Chemical, Metuchen, NJ, USA). A Be^+ peak (first ionization potential = 9.323 eV) is plainly visible on the low mass end of the partial scan (Fig. 5). Peaks for nitrogen (both N^+: 14.534 eV, and $N_2{}^+$) and phosphorous (P^+: 10.487 eV) also appear in the spectrum. The P^+ signal may represent a minor phosphoric acid component in the trace element solution. Phosphorous peaks were also observed during the early stages of this project, when ammonium phosphate was added to the sample during loading in order to stabilize the Th.

As in previous studies [5,17,23], our results demonstrate that the total ion current is dominated by tungsten ions at high temperatures. It is possible that some W^+ ions (7.864 eV) are produced thermally, though some may also be generated via electron impact. In addition to W^+ ions, we also observed significant

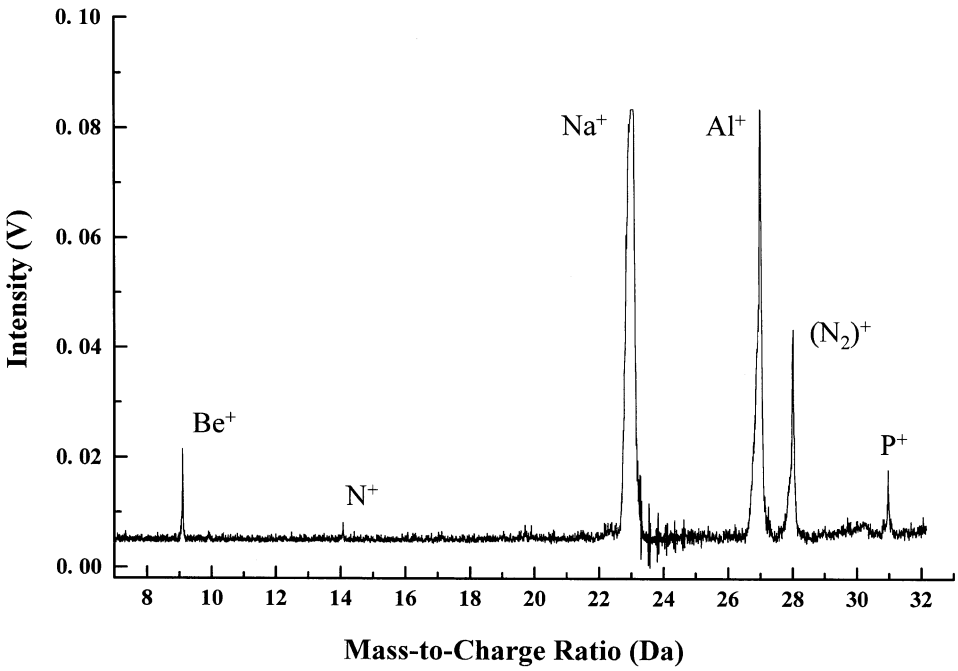

Fig. 5. Mass spectrum obtained at ~1000 °C from a multielement ICPMS mass calibration standard containing 10 ppm beryllium (see text). In addition to Be, peaks corresponding to nitrogen and phosphorous are also readily apparent. Each of these elements has a first ionization potential >9 eV, and is not substantially ionizable via thermal processes alone.

populations of multiply-charged tungsten ions at high temperatures (Fig. 2). The second ionization energy of tungsten is 17.7 eV, thus, W^{2+} (and W^{3+}) ions are not likely to form via thermal processes. If non-thermal ionization mechanisms such as EI are significant, previous models wherein the entire tungsten ion flux originates as a thermally ionized metal vapor within the TIC (e.g. [23]) are, perhaps, in error.

The location of ion formation is also critical, particularly if the TIC method is to be interfaced to a magnetic sector mass analyzer. Electron impact processes may occur within the TIC, at the cavity tip, or some distance from the cavity tip via interactions with the high-energy electrons flowing from the electron bombardment filament. Ion beam focusing in a magnetic sector MS, unlike oa-TOFMS, is sensitive to the location of ion production within the TIMS source. If ions are produced too far in front of the cavity tip, ion beam focusing may be very difficult in a sector instrument without some sort of special lens arrangement.

An additional consideration would be the increased energy spread of EI ions, relative to those produced thermally. Thermal ions typically have low energies, and a low (∼0.2 eV) energy spread [33]. Electron impact ions have a larger energy spread (∼1 eV) [33], and their energies are subject to the voltage gradient in the area where the ions are formed. Thus, the nature of the dominant ionization mechanism in the TIC source (thermal or EI) will govern how the source can be interfaced to the mass analysis system. The contribution of ions via EI also has implications for the quality of isotopic data attainable from TIC-sourced mass spectrometers.

5.2. TIC source performance

Thorium ionization efficiency in a tungsten cavity exceeds that predicted by the Saha–Langmuir equation for thermal ionization at 2300 °C from a flat, polycrystalline tungsten surface (∼0.04%) by ∼30 to ∼75×. This level of ionization efficiency enhancement is similar to that observed for uranium thermionization in a rhenium cavity [16] (relative to a Re filament source in the same sector mass spectrometer), and for Th in a tungsten cavity [17].

Although our data agrees well with that of previous studies [16–18], the maximum ionization efficiency available from the TIC source is probably even greater than the maximum realized (∼3%) during the course of this study. Above ∼1360 °C, thorium metal becomes isostructural with tungsten [34], and Th–W alloys may form at the ionizer surface as a result. Ion losses may also occur within the TOF mass analyzer. Ionization efficiency experiments were repeated using Rb as the analyte ion, an element known to produce thermal ion yields close to 100% at low temperatures. Results from the TIC-TOFMS system indicate that only about 13% of the Rb atoms loaded are detected as ions.

Guilhaus et al. [35] point out that the overall mass analyzer efficiency of a TOFMS (coupled to an ion source having a constant kinetic energy-to-charge ratio) is a function of duty cycle, analyzer transmission, and detector efficiency. By contrast, the purpose of this study is to ascertain the practical ionization efficiency of the TIC-TOFMS system, therefore, only the duty cycle was considered in our ionization efficiency calculations. In fact, the detection efficiency of the chevron-stacked microchannel plate detector used in the TIC-TOFMS corresponds to its 'open area ratio', specified at 59% [36]. The analyzer transmission is largely a function of the grid transmission, and the number of grids [35,37]. Guilhaus et al. [35] formulated an expression for the overall mass-analyzer efficiency, which takes the combined ion losses due to detector efficiency, analyzer transmission and duty cycle into account:

$$F = T_G Y_{det} l_p f \left(\frac{m}{2zeV_{beam}} \right)^{1/2}, \quad (8)$$

where T_G is the product of the grid transmissions (for two grids with 80% transmission, $T_G = 0.64$), Y_{det} the detector yield (0.59), l_p is the detectable length of the ion beam sampled to create an ion packet (=0.0127 m), f the acceleration frequency (Hz), m ion mass (kg), z the number of charges on the ion, e the electron charge ($= 1.6 \times 10^{-19}$ C), and V_{beam} is the velocity of the ion

beam in the accelerating region. For 1 eV Th^+ ions, $V_{beam} = 9.09 \times 10^2$ m/s. The product:

$$l_p f \left(\frac{m}{2zeV_{beam}} \right)^{1/2} \quad (9)$$

is equivalent to the TOFMS sampling duty cycle used in the calculation of ionization efficiency. Taking ion detection efficiency and the analyzer transmission efficiency into account, the overall mass-analyzer efficiency is ~0.73%. Thus, 38% of the ions presented for mass analysis are either lost to the grids, or to the inter-channel web area of the multi-channel plate detector.

Further ion losses may also take place within the electron shielding can, and to the surfaces of the focusing plates. Ion losses inside the electron shielding can are difficult to estimate. If the ion beam is radially symmetrical with respect to Th ion distribution, the area of each focusing plate coated with ion beam residues after a sample run can be used to infer the percentage of the ion beam stopped by the plate. The ratio of the area of iridescent coatings left on the plates after a run to the area of the focusing plate orifices indicates that 10–20% of the ion beam was stopped by each focusing plate. Thus, ion beam interactions with the focusing plates may result in a 19–36% reduction in total ion flux into the accelerating region.

In the context of our work using the TIC-TOFMS, ion losses to focusing plates, TOF grids and the inter-channel web area of the detector are unavoidable. However, future work using different mass analysis systems (quadrupole, magnetic sector) may well yield further improvements to the ionization efficiency of the TIC source.

5.3. Sample vaporization and cluster effects

The painstaking work of Edwards et al. [13] revealed a strong correlation between the amount of sample loaded and the effective ionization efficiency. Edwards et al. [13] observed this trend over a very large Th concentration range: 0.04–200 ng (about 1×10^{12} to 5×10^{14} Th atoms). Using a laser-assisted ionization technique (continuous-wave resonance ionization) to enhance ion populations in the vicinity of a conventional multiple-filament thermal ion source, Johnson and Fearey [38] also observed concentration-dependent thorium ionization efficiency over a very wide range of sample loadings (25–2400 ng Th). However, the magnitude of the variation observed by Johnson and Fearey was miniscule compared to that seen by Edwards et al. [13]. Our study of thorium ionization efficiency using the TIC source over a 0.075–25 ng concentration range revealed little, if any, systematic correlation between sample size and ionization efficiency. Though ionization efficiency measurements are approximations subject to any number of variables, both instrument- and sample-related, the 100-fold increase in Th ionization efficiency documented previously [13] is significant. Though TIC IE measurements at the low end of the concentration range may be compromised somewhat by relatively high thorium blanks, ionization efficiencies from the TIC source (Table 3) vary little relative to those observed for filament ionization over a similar concentration range (Table 1).

Majidi et al. [39] has pointed out that the response of an element during analysis by graphite furnace-atomic absorption spectroscopy (GF-AAS) may also change with decreasing sample size. The thrust of Majidi's argument is that the physical properties of a bulk sample will be different than those of a particle composed of a few hundred, or a few thousand, atoms. In these very small particles, a larger proportion of the constituent atoms reside at the particle surface. Surface atoms have fewer adjacent atoms, and are both more weakly bound and less constrained in their thermal motion than atoms in the bulk [40]. Many investigators [40–45] have documented significant and systematic deviations from bulk physical and chemical behavior in very small particles. Buffat and Borel [46] observed a systematic decrease in the melting temperature of metallic Au with decreasing particle size: from 1609 °C (bulk) to 1570 °C (15 nm cluster of $\sim 10^5$ atoms) to 973 °C (a 2 nm cluster of $\sim 10^2$ atoms). Others [47,48] have documented similar behavior in Ar clusters, and CdS nanocrystals, respectively. It is plausible, then, that particle-size effects could also impact

the atomization (and, hence, the ionization) of an element during TIMS or GF-AAS analysis.

For their experiments, Edwards et al. [13] loaded between 1×10^{12} to 5×10^{14} Th atoms onto a flat, polycrystalline rhenium surface. Typically, thorium is loaded as a nitrate solution, and dried on top of a layer of colloidal graphite which sits on the surface of a carburized rhenium filament. On a 0.1 cm wide rhenium filament, we assume a 1 μL thorium nitrate solution droplet will have a hemispherical profile, but will cover a rectangular area of about $0.025\,cm^2$. A full monolayer of thorium nitrate pentahydrate ($Th(NO_3)_4{\cdot}5H_2O$, Fdd2, $z = 8$) that covers the same area will contain between $\sim 8 \times 10^{10}$ and $\sim 2 \times 10^{11}$ thorium atoms. Thus, even the smallest thorium loadings [13] could conceivably form a continuous monolayer of thorium nitrate pentahydrate underneath the area covered by the original solution droplet. However, if numerous nucleation sites occur across the filament surface, it is possible that the solution could dry as numerous tiny particles. Furthermore, the volume of the $Th(NO_3)_4{\cdot}5H_2O$ film (or particles) is drastically reduced upon heating inside the TIMS source, as the original compound dehydrates and denitrifies to form an oxide [49,50] which is, in turn, reduced to Th metal in the presence of excess carbon. Hussein and Ismail [49] also observed nanometer-scale porosity in ThO_2 obtained via the calcination of $Th(NO_3)_4{\cdot}5H_2O$ in air.

For metallic gold, a melting point depression of about 7.7% can be seen in particles 10 nm in diameter [46]. Particles in this size range contain about 4000 gold atoms. The size distribution of thorium metal particles dispersed on the rhenium TIMS filament prior to vaporization has not yet been characterized, nor have the melting point depression curves for thorium nanoparticles. It seems likely, however, that particle size distribution plays some role in the enhancement of ionization efficiency with decreasing sample size.

The results of our study suggest that, over a similar concentration range, sample size effects [13] are suppressed in cavity-type sources. Ionization efficiencies for nanogram-size thorium samples are similar to those obtained for microgram-size samples [17]. If ionization efficiency for resistively-heated filament TIMS sources is due to melting point depression in nano-sized particles, the dampening of these effects in cavity-type ion sources may well shed additional light on the relevant vaporization and ionization processes in both configurations.

6. Conclusions

Thorium ionization efficiency in the tungsten cavity ion source (1–3%) routinely exceeds that predicted by the Saha–Langmuir equation for the thermal ionization of Th (at 2200 °C) from a flat, polycrystalline tungsten surface by ∼30–75×. This also represents a 10× improvement over typical ionization efficiencies for thorium from a conventional, resistively heated Re filament TIMS ion source. Trace uranium and thorium impurities are present in the tungsten used to fabricate the cavities, and a careful assessment of the Th analytical blank is required for the measurement of samples containing <0.1–25 ng of thorium. A significant proportion of the thorium ion signal (13–40%) at 75–250 pg of Th is contributed by the TIC and, perhaps, the materials used to load the thorium solution into the TIC. Ion signal degrades after approximately ∼60–80 min of operation at high temperatures (≥2200 °C), due to the accumulation of electrically-conductive, vapor-deposited metal films on the insulating support posts that hold the focusing plates and the shielding can.

The presence of singly-, doubly-, and triply-charged tungsten species confirms the existence of electrons of sufficient energy to cause direct ionization. Though electron impact likely occurs within the cavity, the electron bombardment filament used to heat the TIC is a significant source of high-energy electrons which may directly induce ionization via electron impact at, or near, the TIC orifice. For this study, we have not made any distinctions between true thermal ions, and those produced via other processes, such as electron impact. Therefore, the ionization efficiency data presented here, and in previous studies, may not correspond to a purely thermal mechanism. Until

populations of thermal and non-thermal ions of a given element can be characterized for a given set of conditions, the fundamental aspects of ionization in a hot cavity will remain open to question.

Acknowledgements

The ion source was fabricated in the C-Division Machine Shop at LANL by Art Montoya, Joe Hauser and Bob Meir. ICPMS analyses were done by Chris Brink (LANL). Drs. Jose Olivares (LANL), Steve Schubert (NN-20), E. Phil Chamberlin (Chamberlin Enterprises), and Maj. Juan Cuadrado (U.S. Army and LANL) provided valuable assistance and advice. Funding was supplied by the National Nuclear Security Administration (NNSA) Office of Nonproliferation Research and Engineering (NN-20), Proliferation Detection Program, and by the Nuclear Materials and Stockpile Support Capability Development Program at Los Alamos National Laboratory. Los Alamos National Laboratory is operated by the University of California for the U.S. Department of Energy under contract number W-7406-ENG-36. This publication is LA-UR-015070.

References

[1] G.J. Beyer, E. Herrmann, A. Piotrowski, V.J. Raiko, H. Tyrroff, Nucl. Instrum. Meth. 96 (1971) 437.
[2] G.J. Beyer, E. Herrmann, F. Molnar, V.J. Raiko, H. Tyrroff, Radiochem. Radioanal. Lett. 12 (1972) 259.
[3] P.G. Johnson, A. Bolson, C.M. Henderson, Nucl. Instrum. Meth. 106 (1973) 83.
[4] V.A. Karnaukhov, D.D. Bogdanov, A.V. Demyanov, G.I. Koval, L.A. Petrov, Nucl. Instrum. Meth. 120 (1974) 69.
[5] R. Kirchner, Nucl. Instrum. Meth. 186 (1981) 275.
[6] R. Kirchner, Particle Acceleration 47 (1994) 127.
[7] P. Van Duppen, P. Decrock, M. Huyse, R. Kirchner, Rev. Sci. Instrum. 63 (1992) 2381.
[8] V.P. Afanas'ev, V.A. Obukhov, V.I. Raiko, Nucl. Instrum. Meth. 145 (1977) 533.
[9] R. Kirchner, A. Piotrowski, Nucl. Instrum. Meth. 153 (1978) 291.
[10] E.H. Pilzer, G. Engler, Nucl. Instrum. Meth. Phys. Res. B26 (1987) 218.
[11] J.H. Chen, G.J. Wasserburg, Anal. Chem. 53 (1981) 2060.
[12] D.J. Rokop, R.E. Perrin, G.W. Knobeloch, V.M. Armijo, W.R. Shields, Anal. Chem. 54 (1982) 957.
[13] R.L. Edwards, J.H. Chen, G.J. Wasserburg, Earth Planet. Sci. Lett. 81 (1986/1987) 175.
[14] S.J. Goldstein, M.T. Murrell, D.R. Janecky, Earth Planet. Sci. Lett. 96 (1989) 134.
[15] R. Kirchner, Nucl. Instrum. Meth. Phys. Res. A292 (1990) 203.
[16] J. Cesario, Y. Boulin, B. Landeau, Int. J. Mass Spectrom. Ion Phys. 46 (1983) 35.
[17] Y. Duan, E.P. Chamberlin, J.A. Olivares, Int. J. Mass Spectrom. Ion Processes 161 (1997) 27.
[18] Y. Duan, R.E. Danen, X. Yan, R.E. Steiner, J. Cuadrado, D.M. Wayne, V. Majidi, J.A. Olivares, J. Am. Soc. Mass Spectrom. 10 (1999) 1008.
[19] J.M. Kelley, D.M. Robertson, Anal. Chem. 57 (1985) 124.
[20] D.M. Wayne, W. Hang, D.K. McDaniel, R.E. Fields, E. Rios, V. Majidi, Spectrochim. Acta Part B 56 (2001) 1175.
[21] L. Latuszynski, V.I. Raiko, Nucl. Instrum. Meth. 125 (1975) 61.
[22] M. Huyse, Nucl. Instrum. Meth. 215 (1983) 1.
[23] S.J. Goldstein, M.T. Murrell, D.R. Janecky, J.R. Delaney, D.J. Clague, Earth Planet. Sci. Lett. 109 (1992) 255.
[24] M. Roy-Barman, H. Chen, G.J. Wasserburg, Earth Planet. Sci. Lett. 139 (1996) 351.
[25] M.R. Reid, F.C. Ramos, Earth Planet. Sci. Lett. 138 (1996) 67.
[26] C.J. Hawkesworth, S.P. Turner, F. McDermott, D.W. Peate, P. vanCalsteren, Science 276 (1997) 551.
[27] F. Chabaux, A.S. Cohen, R.K. O'Nions, J.R. Hein, Geochim. Cosmochim. Acta 59 (1995) 633.
[28] R.L. Edwards, H. Cheng, M.T. Murrell, S.J. Goldstein, Science 276 (1997) 782.
[29] A. Kaufman, G.J. Wasserburg, D. Porcelli, M. BarMatthews, A. Ayalon, L. Halicz, Earth Planet. Sci. Lett. 156 (1998) 141.
[30] H. Cheng, J. Adkins, R.L. Edwards, E.A. Boyle, Geochim. Cosmochim. Acta 64 (2000) 2401.
[31] D.H. Smith, J.A. Carter, Int. J. Mass Spectrom. Ion Phys. 40 (1981) 211.
[32] T.M. Esat, Int. J. Mass Spectrom. Ion Processes 148 (1995) 159.
[33] I.W. Drummond, Vacuum 34 (1984) 51.
[34] Crystal Structures and Lattice Parameters of Allotropes of the Elements, CRC Handbook of Chemistry and Physics, 2000, in: D.R. Lide, Editor-in-Chief, 3rd Electronic Edition, http://www.knovel.com/knovel2/Toc.jsp?SpaceID=10093&BookID=34, Section 12, pp. 19–21, CRC Press, Inc., Boca Raton, FL, USA.
[35] M. Guilhaus, D. Selby, V. Mlynski, Mass Spec. Rev. 19 (1995) 65.
[36] Burle Technologies, Technical Information Sheet, Long-Life™ Microchannel Plates, 2001, 11 p., Burle Technologies, Inc., Sturbridge, MA, USA, http://www.burle.com/cgi-bin/byteserver.pl/pdf/tp181.pdf
[37] M. Guilhaus, Spectrochim. Acta Part B 55 (2000) 1511.
[38] S.G. Johnson, B.L. Fearey, Spectrochim. Acta Part B 48 (1993) 1065.
[39] V. Majidi, R.G. Smith, R.E. Bossio, R.T. Pogue, M.W. McMahon, Spectrochim. Acta Part B 51 (1996) 941.

[40] M. Schmidt, R. Kusche, B. von Issendorff, H. Haberland, Nature 393 (1998) 238.
[41] R.S. Berry, Sci. Am. 263 (1990) 50.
[42] R.W. Siegel, Phys. Today 10 (1993) 64.
[43] X. Yu, P.M. Duxbury, Phys. Rev. B 52 (1995) 2102.
[44] S.L. Lai, J.Y. Guo, V. Petrova, G. Ramanath, L.H. Allen, Phys. Rev. Lett. 77 (1996) 99.
[45] C. Nutzenadel, A. Zuttel, D. Chartouni, G. Schmid, L. Schlapbach, Eur. Phys. J. D 8 (2000) 245.
[46] P. Buffat, J.P. Borel, Phys. Rev. A 13 (1976) 2287.
[47] M.Y. Hahn, R.L. Whetten, Phys. Rev. Lett. 61 (1988) 1190.
[48] A.N. Goldstein, C.M. Echer, A.P. Alivisatos, Science 256 (1992) 1425.
[49] G.A.M. Hussein, H.M. Ismail, Colloids Surfaces A 99 (1995) 129.
[50] S. Dash, M. Kamruddin, P.K. Ajikumar, A.K. Tyagi, B. Raj, S. Bera, S.V. Narasimhan, J. Nucl. Mat. 278 (2000) 173.